Available online at www.sciencedirect.com
SCIENCE DIRECT®
PERGAMON
Computers and Structures 81 (2003) 1311–1327
Computers & Structures
www.elsevier.com/locate/compstruc

An analytical solution for in-plane free vibration and stability of loaded elliptic arches

K.Y. Nieh [a], C.S. Huang [b,*], Y.P. Tseng [c]

[a] Department of Civil Engineering, Tamkang University, Tamsui 25137, Taiwan
[b] Department of Civil Engineering, National Chiao Tung University, 1001 Ta-Hsueh Rd., Hsinchu 30050, Taiwan
[c] Do & Find Engineering Consultant Co., Ltd., No. 19, Lane 30, Deng Kung Rd., Tamsui 251, Taiwan

Received 30 September 2002; accepted 10 January 2003

Abstract

In-plane free vibration and stability analyses of elliptic arches subjected to a uniformly distributed vertical static loading are performed here. A variational principle is applied to derive the governing equations for free vibration and stability of preloaded arches, considering the effect of the extensibility of the arch centerline but neglecting the effect of shear deformation. Particular attention is given to present a general procedure for combining series solutions with stiffness matrixes to construct an analytical solution for free vibration and stability of loaded arches with varying curvature. The correctness of the proposed solution is verified through a convergence study on the vibration frequencies of a loaded circular arch and by comparing the results with published data. The solution is further applied to investigate the behaviors of clamped or fixed–free elliptic arches.

Keywords: Analytical solution; In-plane; Vibration; Stability; Arch; Varying curvature

1. Introduction

Curved beams are important structural elements in civil, mechanical and aerospace engineering applications, such as bridges, roof structures, springs, and stiffeners in aircraft structures. Due to their importance, the literature on the dynamic behavior of planar curved structural elements is vast. The related work can be traced back to the 19th century [1]. Survey studies on the dynamic analysis of arch-type structures have been compiled in references [2–4], where more than 500 articles have been reviewed. Most of the previous research has principally dealt with the dynamic analysis of unloaded arch-type structures. This paper presents a study on the vibration behaviors of elliptic arches under static and uniformly distributed loading.

Rather little previous work has dealt with the vibration and stability analysis of statically loaded arches even though dynamic analyses of loaded arches are frequently needed in many engineering applications, such as arch bridges, where arches are subjected to their own weights or the static loading from the bridge deck. All of the previous studies concentrated to circular arches, and most of them assumed an in-extensional centerline for the sake of simplicity. For example, Timoshenko and Gere [5] and Simitses [6] showed closed solutions for the stability of simply supported or clamped circular arches subjected to uniformly distributed radial forces. Gjelsvik and Bonder [7] utilized an energy approach to investigate the stability of a clamped arch under center point loads. Schreyer and Masur [8] established a closed-form general solution to the stability problem of an arch subjected to uniformly distributed loading and having

* Corresponding author. Tel.: +886-3-5712121x54962; fax: +886-3-5716257.
E-mail address: cshuang@mail.nctu.edu.tw (C.S. Huang).

0045-7949/03/$ - see front matter © 2003 Elsevier Science Ltd. All rights reserved.
doi:10.1016/S0045-7949(03)00057-9

various boundary conditions. Wasserman [9] developed exact and approximate formulae for determining the lowest natural frequencies and critical loads of arches with flexibly supported ends. In Kang et al. [10], the differential quadrature method was used to find the critical loads of circular arches.

Lin and Soedel [11] showed that centerline extensibility significantly influences the vibrations of rotating thick rings. Using the Ritz method, Chidamparam and Leissa [12] first analyzed the in-plane free vibrations of loaded circular arches with consideration of an the extensible centerline. However, they determined the distribution of the initial axial forces based on the assumption of an in-extensional centerline. Chidamparam and Leissa [12] concluded that centerline stretching in the vibratory motion results in a decrease of the vibration frequency, and that this decrease may be very considerable, especially for shallow arches. Discarding the assumption of an in-extensional centerline used by Chidamparam and Leissa [12], Huang and Nieh [13] further developed an analytical solution for vibrations of circular arches under static, uniformly distributed loading. Comparing the results of Chidamparam and Leissa [12] with those of Huang and Nieh [13] reveals considerable differences for shallow arch cases with large compressive or tensile loading.

This paper presents the vibration and stability analysis of statically loaded arches with varying curvature. The governing equations are developed from the variational form given by Washizu [14] for the dynamic problems of an elastic body with initial stresses. In the derivation of the equations, centerline extensibility but no shear deformation is considered. A general analytical solution to the governing equations is obtained by decomposing the entire arch under consideration into several sub-domains and establishing a stiffness matrix for each sub-domain. The stiffness matrix is developed according to a series solution of the governing equations defined in the sub-domain. The proposed solution is verified through a convergence study on vibration frequencies for a loaded circular arch, and through comparison of the present results with published data. The proposed solution is applied to investigate the effects of the opening angle (θ_0), the ratio of the long-axis length to the short-axis length (a/b), and the ratio of the twice long-axis length to the radius of gyration of the cross-section area (μ) on the vibration frequencies and buckling loads of elliptic arches under uniformly distributed vertical forces.

2. Governing equations

For the arch with opening angle θ_0 shown in Fig. 1, the radius of the centroidal axis, denoted by R, is a function of the angular co-ordinate, denoted by θ, measured from the middle of the arch. The arch cross-section is assumed to have at least one symmetry axis, so the in-plane motion of the arch does not couple with out-of-plane motion. The arch is subjected to static external forces along the tangential and normal directions with the intensities P_t and P_n, respectively, which produce initial stresses $\sigma_{ij}^{(0)}$ in equilibrium. It is assumed that the resulting static deformation is small enough so that the changes in the geometry of the arch can be neglected. For in-plane free vibration, the dynamic tangential and radial displacements of a point with coordinates (r,θ) are denoted by $\bar{v}$ and $\bar{w}$, respectively. The sign conventions for positive dynamic displacement components, moment (M), shear force (Q), and axial force (N) are also given in Fig. 1.

Ignoring shear deformation yields the in-plane displacement field of an arch as

$$\bar{v}(r,\theta,t) = v(\theta,t) - z\left(\frac{\partial w}{\partial S} - v\right), \qquad \bar{w}(r,\theta,t) = w(\theta,t), \tag{1}$$

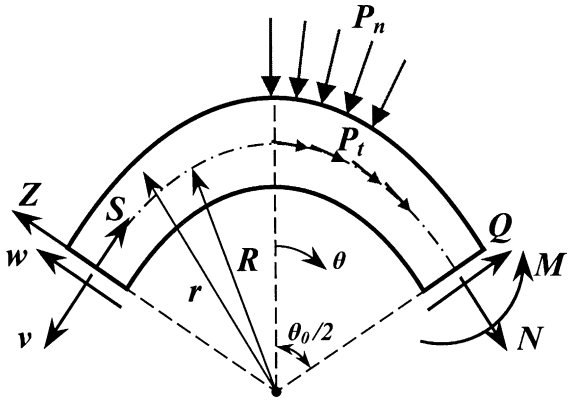

Fig. 1. Arch coordinates and displacement and stress resultants for in-plane motion.

where v and w represent the tangential and radial displacements of the centroidal axis, respectively, $z = r - R$, and S is the arc length coordinate.

To derive the governing equations of free vibration for a loaded arch and the associated boundary conditions, we use the variational principle for the dynamic problem of an elastic body with equilibrium initial stresses, which was derived by Washizu [14] via the principle of virtual work:

$$\delta \int_{t_1}^{t_2} \left\{ T - U - \int\int_V \int \sigma_{ij}^{(0)} \varepsilon_{ij}^{(H)} \, \mathrm{d}V \right\} \mathrm{d}t = 0, \tag{2}$$

where T and U are the kinetic and strain energy, given by

$$T = \int\int_V \int \frac{1}{2} \rho (\dot{\bar{v}}^2 + \dot{\bar{w}}^2) \, \mathrm{d}V, \tag{3a}$$

$$U = \int\int_V \int \frac{1}{2} \sigma_{ij} \varepsilon_{ij}^{(L)} \, \mathrm{d}V. \tag{3b}$$

$\varepsilon_{ij}^{(L)}$ and $\varepsilon_{ij}^{(H)}$ are infinitesimal strain components and high-order strain components, respectively, σ_{ij} represents dynamic stress components, ρ is the material density, and the dot denotes the derivative with respect to time. In Eq. (2), the body subjected to the static loading is considered as the reference state, which is the state before the start of a dynamic deformation of interest.

For the displacement field given by Eq. (1), the non-vanishing strain component is axially normal strain; hence

$$\varepsilon_{\theta\theta}^{(L)} = \frac{1}{r} (\bar{v}' + \bar{w}), \tag{4a}$$

$$\varepsilon_{\theta\theta}^{(H)} = \frac{1}{2r^2} (w' - v)^2. \tag{4b}$$

The prime represents the differential with respect to θ. In Eq. (4b), small strain but moderately small rotation is assumed.

By assuming sufficiently small h/R (where h is the thickness of the arch), by neglecting rotary inertia, and by using the stress–strain relation $\sigma_{\theta\theta} = E\varepsilon_{\theta\theta}^{(L)}$, where E is the elastic modulus, we can derive the following governing equations from Eqs. (2)–(4) by carrying out a typical variation process [15]:

$$-\frac{1}{R} \frac{\partial M}{\partial S} + \frac{\partial N}{\partial S} + \frac{N^{(0)}}{R} \left(\frac{\partial w}{\partial S} - \frac{v}{R} \right) = \rho A \ddot{v}, \tag{5a}$$

$$-\left(\frac{\partial^2 M}{\partial S^2} + \frac{N}{R} \right) + \frac{\partial}{\partial S} \left(N^{(0)} \left(\frac{\partial w}{\partial S} - \frac{v}{R} \right) \right) = \rho A \ddot{w} \tag{5b}$$

and the following associated boundary conditions:

Natural boundary condition	
N	
$\frac{\partial M}{\partial S} + N^{(0)} \left(\frac{\partial w}{\partial S} - \frac{v}{R} \right)$	(6)
M	
Essential boundary condition	
v	
w	
$\frac{\partial w}{\partial S} - \frac{v}{R}$	

where $N^{(0)}$ is the initial axial force and A is the cross-sectional area.

In deriving Eqs. (5) and (6), the following definition of the stress resultants is introduced:

$$(N, M) = \int_A \sigma_{\theta\theta}(1, z)\, \mathrm{d}A. \tag{7}$$

Consequently, from Eq. (4a) and the stress–strain relation, we can express the stress resultants in terms of displacement components as follows:

$$N = EA\left(\frac{\partial v}{\partial S} + \frac{w}{R}\right), \tag{8a}$$

$$M = EI\left[\frac{\partial^2 w}{\partial S^2} - \frac{\partial}{\partial S}\left(\frac{v}{R}\right)\right], \tag{8b}$$

where I is the second moment of the arch cross-section about the centerline. Notably, when shear deformation is neglected, the shear force does not appear in the variational principle of Eq. (2), so the resulting governing equations and the associated boundary conditions do not involve terms with the shear force. Nevertheless, it is well-known that the shear force is related to the moment through the following equilibrium equation:

$$\frac{\partial M}{\partial S} + Q = 0. \tag{9}$$

Substituting Eqs. (8a) and (8b) into Eqs. (5a) and (5b) and introducing the dimensionless $\tilde{v} = v/L$, $\tilde{w} = w/L$ and $\bar{R} = R/L$, where L is a characteristic length of the arch, yield

$$\tilde{w}''' + \tilde{\alpha}_1\tilde{w}'' + \tilde{\alpha}_2\tilde{w}' + \tilde{\alpha}_3\tilde{w} + \tilde{\beta}_1\tilde{v}'' + \tilde{\beta}_2\tilde{v}' + \tilde{\beta}_3\tilde{v} = -\frac{\rho\bar{R}L^2}{E\bar{\gamma}^2\xi^3}\ddot{\tilde{v}}, \tag{10a}$$

$$\tilde{v}''' + \tilde{\beta}_4\tilde{v}'' + \tilde{\beta}_5\tilde{v}' + \tilde{\beta}_6\tilde{v} + \tilde{\alpha}_4\tilde{w}^{iv} + \tilde{\alpha}_5\tilde{w}''' + \tilde{\alpha}_6\tilde{w}'' + \tilde{\alpha}_7\tilde{w}' + \tilde{\alpha}_8\tilde{w} = \frac{\rho L^2\bar{R}}{E\bar{\gamma}^2\xi^3}\ddot{\tilde{w}}, \tag{10b}$$

where

$$\begin{aligned}
&\tilde{\alpha}_1 = \frac{3\xi'}{\xi}, \quad \tilde{\alpha}_2 = \frac{\xi''}{\xi} + \left(\frac{\xi'}{\xi}\right)^2 - \frac{1}{\xi^2}\left(\frac{1}{\bar{\gamma}^2} + \frac{L^2N^{(0)}}{EI}\right),\\
&\tilde{\alpha}_3 = \frac{\bar{R}'}{\bar{\gamma}^2\bar{R}\xi^2}, \quad \tilde{\alpha}_4 = -\bar{R}\xi, \quad \tilde{\alpha}_5 = -6\bar{R}\xi',\\
&\tilde{\alpha}_6 = -\bar{R}\left[4\xi'' + \frac{7(\xi')^2}{\xi} - \frac{L^2N^{(0)}}{EI\xi}\right],\\
&\tilde{\alpha}_7 = -\bar{R}\left[\xi''' + \frac{4\xi'\xi''}{\xi} + \frac{(\xi')^3}{\xi^2} - \frac{L^2N^{(0)}\xi'}{EI\xi^2} - \frac{L^2(N^{(0)})'}{EI\xi}\right],\\
&\tilde{\alpha}_8 = -\frac{1}{\gamma^2\bar{R}\xi^3},\\
&\tilde{\beta}_1 = -\frac{1}{\xi}\left(\frac{1}{\bar{R}} + \frac{\bar{R}}{\bar{\gamma}^2}\right), \quad \tilde{\beta}_2 = -\frac{\xi'}{\xi^2}\left(\frac{1}{\bar{R}} + \frac{\bar{R}}{\bar{\gamma}^2}\right) + \frac{2\bar{R}'}{\bar{R}^2\xi},\\
&\tilde{\beta}_3 = \frac{1}{\bar{R}^2}\left(\frac{\bar{R}''}{\xi} + \frac{\bar{R}'\xi'}{\xi^2}\right) - \frac{2(\bar{R}')^2}{\bar{R}^3\xi} + \frac{N^{(0)}L^2}{\bar{R}EI\xi^3},\\
&\tilde{\beta}_4 = -\left[-\frac{3\xi'}{\xi} + \frac{3\bar{R}'}{\bar{R}}\right],\\
&\tilde{\beta}_5 = -\left[\frac{6\bar{R}'}{\bar{R}}\frac{\xi'}{\xi} - \frac{\xi''}{\xi} - \left(\frac{\xi'}{\xi}\right)^2 + \frac{3\bar{R}''}{\bar{R}} - 6\left(\frac{\bar{R}'}{\bar{R}}\right)^2 + \frac{1}{\bar{\gamma}^2\xi^2} + \frac{N^{(0)}L^2}{EI\xi^2}\right],\\
&\tilde{\beta}_6 = -\left\{\frac{\bar{R}'''}{\bar{R}} + \frac{3\bar{R}''}{\bar{R}}\frac{\xi'}{\xi} - \frac{6\bar{R}'\bar{R}''}{\bar{R}^2} - \left(\frac{\bar{R}''}{\bar{R}}\right)^2\frac{\xi'}{\xi} + 6\left(\frac{\bar{R}'}{\bar{R}}\right)^3 + \frac{\bar{R}'}{\bar{R}}\left[\frac{\xi''}{\xi} + \left(\frac{\xi'}{\xi}\right)^2\right] + \frac{L^2(N^{(0)})'}{EI\xi^2} - \frac{L^2N^{(0)}}{EI\xi^2}\frac{\bar{R}'}{\bar{R}}\right\},\\
&\xi = \frac{\mathrm{d}S}{L\,\mathrm{d}\theta}, \quad \bar{\gamma}^2 = I/(L^2A).
\end{aligned} \tag{11}$$

Notably, Eqs. (10a) and (10b) can be reduced to the governing equations used by Chidamparam and Leissa [12] for analyzing the vibrations of loaded circular arches.

3. Method of solution

Apparently, to solve Eqs. (10a) and (10b), we have to know the distribution of axial forces along an arch under static external forces. Then, the vibration frequencies or the bulking loads can be determined for the arch. Here, a series solution combined with the stiffness matrix approach is applied to establish analytical solutions for static and dynamic responses.

3.1. Solution for $N^{(0)}$

For an arch with varying curvature subjected to in-plane static loading, the equations governing the deformation are similar to Eqs. (10a) and (10b). They are

$$\hat{w}''' + \tilde{\alpha}_1\hat{w}'' + \hat{\alpha}_2\hat{w}' + \tilde{\alpha}_3\hat{w} + \tilde{\beta}_1\hat{v}'' + \tilde{\beta}_2\hat{v}' + \hat{\beta}_3\hat{v} = \frac{\bar{R}L^3}{EI\xi^3}P_{\mathrm{t}}, \tag{12a}$$

$$\hat{v}''' + \tilde{\beta}_4\hat{v}'' + \hat{\beta}_5\hat{v}' + \hat{\beta}_6\hat{v} + \tilde{\alpha}_4\hat{w}^{iv} + \tilde{\alpha}_5\hat{w}''' + \hat{\alpha}_6\hat{w}'' + \hat{\alpha}_7\hat{w}' + \tilde{\alpha}_8\hat{w} = \frac{\bar{R}L^3}{EI\xi^3}P_{\mathrm{n}}, \tag{12b}$$

where $\hat{\alpha}_i$ ($i = 2$, 6 and 7) and $\hat{\beta}_j$ ($j = 3$, 5 and 6) are identical to $\tilde{\alpha}_i$ and $\tilde{\beta}_j$ with $N^{(0)} = 0$, respectively; $\hat{v}$ and $\hat{w}$ are analogous to $\tilde{v}$ and $\tilde{w}$, respectively, and are the dimensionless static displacement components; P_{t} and P_{n} are the distributed loads along the tangential and normal directions, respectively (see Fig. 1).

Eqs. (12a) and (12b) are two ordinary differential equations with variable coefficients. It is generally impossible to find a closed-form solution for these two equations. Nevertheless, the famous Frobenius method can be applied to construct an analytical solution in terms of a power series of θ. Each variable coefficient and external loading function in Eqs. (12a) and (12b) has to be expressed in terms of a Taylor's expansion series as follows:

$$\begin{aligned}
&\tilde{\alpha}_1 = \sum_{k=0,1}^{K} a_k(\theta-\eta)^k, \quad \hat{\alpha}_2 = \sum_{k=0,1}^{K} b_k(\theta-\eta)^k,\\
&\tilde{\alpha}_3 = \sum_{k=0,1}^{K} c_k(\theta-\eta)^k, \quad \tilde{\alpha}_4 = \sum_{k=0,1}^{K} d_k(\theta-\eta)^k,\\
&\tilde{\alpha}_5 = \sum_{k=0,1}^{K} e_k(\theta-\eta)^k, \quad \hat{\alpha}_6 = \sum_{k=0,1}^{K} f_k(\theta-\eta)^k,\\
&\hat{\alpha}_7 = \sum_{k=0,1}^{K} g_k(\theta-\eta)^k, \quad \tilde{\alpha}_8 = \sum_{k=0,1}^{K} h_k(\theta-\eta)^k,\\
&\tilde{\beta}_1 = \sum_{k=0,1}^{K} \bar{a}_k(\theta-\eta)^k, \quad \tilde{\beta}_2 = \sum_{k=0,1}^{K} \bar{b}_k(\theta-\eta)^k,\\
&\hat{\beta}_3 = \sum_{k=0,1}^{K} \bar{c}_k(\theta-\eta)^k, \quad \tilde{\beta}_4 = \sum_{k=0,1}^{K} \bar{d}_k(\theta-\eta)^k,\\
&\hat{\beta}_5 = \sum_{k=0,1}^{K} \bar{e}_k(\theta-\eta)^k, \quad \hat{\beta}_6 = \sum_{k=0,1}^{K} \bar{f}_k(\theta-\eta)^k,\\
&\frac{\bar{R}L^3}{EI\xi^3}P_{\mathrm{t}} = \sum_{k=0,1}^{K} p_k(\theta-\eta)^k, \quad \frac{\bar{R}L^3}{EI\xi^3}P_{\mathrm{n}} = \sum_{k=0,1}^{K} \bar{p}_k(\theta-\eta)^k,
\end{aligned} \tag{13}$$

where η is a reference point along the centroidal axis. The solution of Eqs. (12a) and (12b) is also assumed to be in the following form:

$$\hat{w} = \sum_{j=0,1}^{J} A_j(\theta-\eta)^j \quad \text{and} \quad \hat{v} = \sum_{j=0,1}^{J} B_j(\theta-\eta)^j. \tag{14}$$

Substituting Eqs. (13) and (14) into Eqs. (12a) and (12b) with careful arrangement, we can develop the following recursive equations from the vanishing coefficients of $(\theta-\eta)$ with different powers:

$$A_{i+3} = \frac{1}{(i+3)(i+2)(i+1)}\left\{p_i - \sum_{k=0}^{i}[(k+2)(k+1)a_{i-k}A_{k+2} + (k+1)b_{i-k}A_{k+1} + c_{i-k}A_k + (k+2)(k+1)\bar{a}_{i-k}B_{k+2} + (k+1)\bar{b}_{i-k}B_{k+1} + \bar{c}_{i-k}B_k]\right\}, \tag{15a}$$

$$B_{i+3} = \frac{1}{1-\bar{a}_0 d_0)(i+3)(i+2)(i+1)}\left\{\bar{p}_i - \sum_{k=0}^{i}[(k+2)(k+1)\bar{d}_{i-k}B_{k+2} + (k+1)\bar{e}_{i-k}B_{k+1} + f_{i-k}B_k + (k+3)(k+2)(k+1)e_{i-k}A_{k+3} + (k+2)(k+1)f_{i-k}A_{k+2} + (k+1)g_{i-k}A_{k+1} + h_{i-k}A_k] - \sum_{k=0}^{i-1}[(k+4)(k+3)(k+2)(k+1)d_{i-k}A_{k+4}] - (i+1)d_0\left\{p_{i+1} - \sum_{k=0}^{i+1}[(k+2)(k+1)a_{i-k+1}A_{k+2} + (k+1)b_{i-k+1}A_{k+1} + c_{i-k+1}A_k + (k+1)\bar{b}_{i-k+1}B_{k+1} + \bar{c}_{i-k+1}B_k] - \sum_{k=0}^{i}[(k+2)(k+1)\bar{a}_{i-k+1}B_{k+2}]\right\}\right\}. \tag{15b}$$

Since Eqs. (12a) and (12b) are non-homogeneous differential equations, the general solution consists of a homogeneous solution ($\hat{w}_h$ and $\hat{v}_h$) and a particular solution ($\hat{w}_p$ and $\hat{v}_p$). Hence, we let

$$\hat{w} = \hat{w}_h + \hat{w}_p = \sum_{k=0,1}^{K} A_k^{(h)}(\theta-\eta)^k + \sum_{k=0,1}^{K} A_k^{(p)}(\theta-\eta)^k, \tag{16a}$$

$$\hat{v} = \hat{v}_h + \hat{v}_p = \sum_{k=0,1}^{K} B_k^{(h)}(\theta-\eta)^k + \sum_{k=0,1}^{K} B_k^{(p)}(\theta-\eta)^k. \tag{16b}$$

From Eqs. (15a) and (15b) with p_i and $\bar{p}_i$ equal to zero, the coefficients $A_k^{(h)}$ and $B_k^{(h)}$ with $k \geqslant 3$ are expressed in terms of $A_k^{(h)}$ and $B_k^{(h)}$ with $k = 0$, 1 and 2, where are to be determined by the specified boundary conditions. The coefficients $A_k^{(p)}$ and $B_k^{(p)}$ with $k \geqslant 3$ are determined from Eqs. (15a) and (15b) by setting $A_k^{(p)}$ and $B_k^{(p)}$ with $k \leqslant 2$ equal to 1. Consequently, the solution can be rewritten as

$$\hat{w} = A_0^{(h)}\hat{w}_0 + A_1^{(h)}\hat{w}_1 + A_2^{(h)}\hat{w}_2 + B_0^{(h)}\hat{w}_3 + B_1^{(h)}\hat{w}_4 + B_2^{(h)}\hat{w}_5 + \hat{w}_p, \tag{17a}$$

$$\hat{v} = A_0^{(h)}\hat{v}_0 + A_1^{(h)}\hat{v}_1 + A_2^{(h)}\hat{v}_2 + B_0^{(h)}\hat{v}_3 + B_1^{(h)}\hat{v}_4 + B_2^{(h)}\hat{v}_5 + \hat{v}_p, \tag{17b}$$

where $\hat{w}_i$ and $\hat{v}_i$ $(i = 0, 1, \ldots, 5)$ are polynomials of $(\theta-\eta)$, whose coefficients are determined from Eqs. (15a) and (15b) with p_i and $\bar{p}_i$ equal to zero.

We can use Eqs. (17a) and (17b) to determine the solution that satisfies the specified boundary conditions. Very high-order terms may have to be used to obtain accurate results; however, numerical difficulties typically occur. In addition, the convergence radius of the series solution may not be able to cover the entire arch under consideration. To avoid such possible problems, the finite element concept is introduced into the series solution. The arch is decomposed into several sub-domains. For each sub-domain, a series solution is constructed by following the above procedure and taking η as the middle angle of the sub-domain. The end (or nodal) displacement components (see Fig. 2) for the nth sub-domain can be expressed as

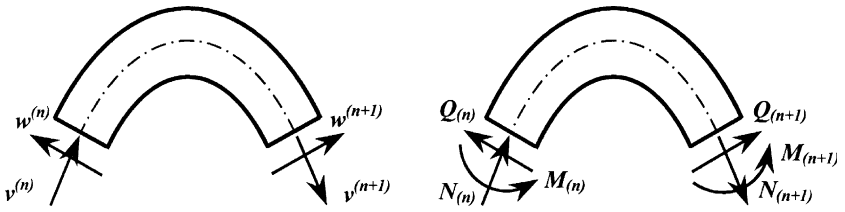

Fig. 2. Positive displacement and stress resultants for the nth element.

$$\begin{Bmatrix} v^{(n)} \\ w^{(n)} \\ w'^{(n)} \\ v^{(n+1)} \\ w^{(n+1)} \\ w'^{(n+1)} \end{Bmatrix} = L \begin{bmatrix} \hat{v}_0(\theta_n) & \hat{v}_1(\theta_n) & \hat{v}_2(\theta_n) & \hat{v}_3(\theta_n) & \hat{v}_4(\theta_n) & \hat{v}_5(\theta_n) \\ \hat{w}_0(\theta_n) & \hat{w}_1(\theta_n) & \hat{w}_2(\theta_n) & \hat{w}_3(\theta_n) & \hat{w}_4(\theta_n) & \hat{w}_5(\theta_n) \\ \hat{w}'_0(\theta_n) & \hat{w}'_1(\theta_n) & \hat{w}'_2(\theta_n) & \hat{w}'_3(\theta_n) & \hat{w}'_4(\theta_n) & \hat{w}'_5(\theta_n) \\ \hat{v}_0(\theta_{n+1}) & \hat{v}_1(\theta_{n+1}) & \hat{v}_2(\theta_{n+1}) & \hat{v}_3(\theta_{n+1}) & \hat{v}_4(\theta_{n+1}) & \hat{v}_5(\theta_{n+1}) \\ \hat{w}_0(\theta_{n+1}) & \hat{w}_1(\theta_{n+1}) & \hat{w}_2(\theta_{n+1}) & \hat{w}_3(\theta_{n+1}) & \hat{w}_4(\theta_{n+1}) & \hat{w}_5(\theta_{n+1}) \\ \hat{w}'_0(\theta_{n+1}) & \hat{w}'_1(\theta_{n+1}) & \hat{w}'_2(\theta_{n+1}) & \hat{w}'_3(\theta_{n+1}) & \hat{w}'_4(\theta_{n+1}) & \hat{w}'_5(\theta_{n+1}) \end{bmatrix} \begin{Bmatrix} A_0^{(h)} \\ A_1^{(h)} \\ A_2^{(h)} \\ B_0^{(h)} \\ B_1^{(h)} \\ B_2^{(h)} \end{Bmatrix}$$

$$+ L \begin{Bmatrix} \hat{v}_p(\theta_n) \\ \hat{w}_p(\theta_n) \\ \hat{w}'_p(\theta_n) \\ \hat{v}_p(\theta_{n+1}) \\ \hat{w}_p(\theta_{n+1}) \\ \hat{w}'_p(\theta_{n+1}) \end{Bmatrix} = [\beta_n]\{\boldsymbol{A}_n\} + \{\boldsymbol{D}_n^{(p)}\}. \tag{18}$$

By using the relations between the stress resultants and displacement components, we can write the end (or nodal) forces (see Fig. 2) in terms of end displacement components as

$$\begin{Bmatrix} N_{(n)} \\ Q_{(n)} \\ M_{(n)} \\ N_{(n+1)} \\ Q_{(n+1)} \\ M_{(n+1)} \end{Bmatrix} = [\hat{\boldsymbol{K}}_n] \begin{Bmatrix} v^{(n)} \\ w^{(n)} \\ w'^{(n)} \\ v^{(n+1)} \\ w^{(n+1)} \\ w'^{(n+1)} \end{Bmatrix} + \{\boldsymbol{f}_n^{(p)}\}, \tag{19}$$

where the lengthy expressions of the stiffness matrix for the nth sub-domain $[\hat{\boldsymbol{K}}_n]$ and the equivalent nodal external force vector $\{\boldsymbol{f}_n^{(p)}\}$ are given in Appendix A. Through the continuity conditions between adjacent sub-domains, we can assemble the relation given in Eq. (19) for each sub-domain to form the following relation for the entire arch:

$$[\boldsymbol{K}]\{\boldsymbol{u}\} = \{\boldsymbol{F}\}, \tag{20}$$

where $[\boldsymbol{K}]$ is the stiffness matrix for the whole arch, and $\{\boldsymbol{u}\}$ and $\{\boldsymbol{F}\}$ are vectors consisting of nodal displacement components and equivalent external nodal forces, respectively.

By satisfying the boundary conditions, we are able to solve for $\{\boldsymbol{u}\}$ using Eq. (20). Then, the coefficients $\{\boldsymbol{A}_n\}$ for each sub-domain can be determined from Eq. (18), and the initial axial force $N^{(0)}(\theta)$ for each sub-domain can be determined.

3.2. Solution for vibration frequencies and buckling loads

For free vibration analysis, the displacement components are assumed to be

$$\tilde{w} = \widetilde{W}\,\mathrm{e}^{\mathrm{i}\omega t} \quad \text{and} \quad \tilde{v} = \widetilde{V}\,\mathrm{e}^{\mathrm{i}\omega t}, \tag{21}$$

where ω is the vibration frequency. Substituting Eq. (21) into Eqs. (10a) and (10b) leads to

$$\widetilde{W}''' + \tilde{\alpha}_1\widetilde{W}'' + \tilde{\alpha}_2\widetilde{W}' + \tilde{\alpha}_3\widetilde{W} + \tilde{\beta}_1\widetilde{V}'' + \tilde{\beta}_2\widetilde{V}' + \bar{\beta}_3\widetilde{V} = 0, \tag{22a}$$

$$\widetilde{V}''' + \tilde{\beta}_4\widetilde{V}'' + \tilde{\beta}_5\widetilde{V}' + \tilde{\beta}_6\widetilde{V} + \tilde{\alpha}_4\widetilde{W}^{iv} + \tilde{\alpha}_5\widetilde{W}''' + \tilde{\alpha}_6\widetilde{W}'' + \tilde{\alpha}_7\widetilde{W}' + \bar{\alpha}_8\widetilde{W} = 0, \tag{22b}$$

where

$$\bar{\alpha}_8 = \tilde{\alpha}_8 + \frac{\rho\bar{R}L^2\omega^2}{E\bar{\gamma}^2\xi^3} \quad \text{and} \quad \bar{\beta}_3 = \tilde{\beta}_3 - \frac{\rho\bar{R}L^2\omega^2}{E\bar{\gamma}^2\xi^3}.$$

The similarity between Eqs. (22a) and (22b) and Eqs. (12a) and (12b) indicates that the procedure for determining the homogeneous solution in the preceding section can be directly applied to construct the general solution of Eqs. (22a) and (22b). For convenience, the sub-domains used here are exactly the same as those used for the static solution. Accordingly, we can develop the following relation for the entire loaded arch:

$$[\widetilde{\boldsymbol{K}}]\{\widetilde{\boldsymbol{U}}\} = \{\widetilde{\boldsymbol{F}}\}, \tag{23}$$

where $[\widetilde{\boldsymbol{K}}]$ is the so-called dynamic stiffness matrix because the inertia forces are included in the right-hand side of Eq. (23), $\{\widetilde{\boldsymbol{U}}\}$ is the vector for the nodal vibratory displacement components, and $\{\widetilde{\boldsymbol{F}}\}$ is a vector having non-zero unknown stress resultants at the nodes on the boundary. Eq. (23) can be further rewritten as

$$\begin{bmatrix} [\widetilde{\boldsymbol{K}}_{uu}] & [\widetilde{\boldsymbol{K}}_{ub}] \\ [\widetilde{\boldsymbol{K}}_{bu}] & [\widetilde{\boldsymbol{K}}_{bb}] \end{bmatrix} \begin{Bmatrix} \{\widetilde{\boldsymbol{U}}_u\} \\ \{\widetilde{\boldsymbol{U}}_b\} \end{Bmatrix} = \begin{Bmatrix} \{\boldsymbol{0}\} \\ \{\widetilde{\boldsymbol{F}}_b\} \end{Bmatrix}, \tag{24}$$

where $\{\widetilde{\boldsymbol{U}}_u\}$ and $\{\widetilde{\boldsymbol{U}}_b\}$ are the unknown nodal displacement components and the prescribed displacement components on the boundaries, respectively, and $\{\widetilde{\boldsymbol{F}}_b\}$ is the unknown stress resultants on the displacement prescribed boundaries. Because $\{\widetilde{\boldsymbol{U}}_b\}$ is a zero vector in a free vibration problem, the natural frequencies for the arch are those ω's resulting in the vanishing determinant of $[\widetilde{\boldsymbol{K}}_{uu}]$. The buckling loads are those external loads that make the free vibration frequencies equal to zero.

4. Convergence study

Careful investigation of the solution methodology given in the previous section reveals that the accuracy of the solution is dependent on the number of sub-domains that an arch is decomposed into, the number of expansion terms for variable coefficients (n_c), and the number of terms used in the series solution (n_s) for each sub-domain. To validate the correctness of the proposed solution, convergence studies were done for clamped circular arches initially loaded with a uniformly distributed vertical load with intensity χ. The arches considered had $h/R = 0.01$ and were symmetric with respect to a vertical line.

In Table 1 are listed the non-dimensional frequency parameters $\omega R^2\sqrt{\rho A/EI}$ of an arch with $\theta_0 = 100°$, subjected to a vertical uniform loading with intensity χ such that $\chi R^3/EI = 20$. The results were obtained using different numbers of sub-domains along with different values of n_c and n_s. Notably, in determining the static solution for $N^{(0)}$, the coefficients of Eqs. (12a) and (12b) were kept constant, and the number of terms in a series solution was chosen equal to n_c as given in Table 1. The results show that for a fixed number of sub-domains, convergent results could be obtained by simultaneously increasing n_c and n_s. If one uses a small number of sub-domains and n_c, then one may obtain incorrect answers even if one uses a very large n_s because the obtained $N^{(0)}$ is not accurate enough. Convergent results can also be obtained by increasing the number of sub-domains with fixed n_c and n_s.

Table 1 also lists the results provided by Huang and Nieh [13], who used a closed-form static solution for $N^{(0)}$ and determined the vibration frequencies by using a series solution along with the dynamic stiffness matrix approach. The agreement of the present convergent results with those given in [13] indicates the correctness of the present solution.

5. Numerical results

Convergent non-dimensional frequency parameters $\lambda = \omega L^2\sqrt{\rho A/EI}$ of elliptic arches with rectangular cross-sections are tabulated in Tables 2 and 3 and plotted in Figs. 3–6 for various conditions. The arches considered were geometrically symmetric to their short axis and subjected to a uniformly distributed vertical loading with intensity χ (see Fig. 7). The radius of the centroidal axis of an elliptic arch is defined as

$$R = \frac{1}{ab}(a^2\cos^2\theta + b^2\sin^2\theta)^{3/2}, \tag{25}$$

Table 1
Convergence of non-dimensional frequency parameters $\omega R^2\sqrt{\rho A/EI}$ for a loaded clamped circular arch with $h/R = 0.01$ and $\theta_0 = 100°$ ($\chi R^3/EI = 20$)

Element no.	Mode no.	n_c	n_s				Ref. [13]
			10	15	20	30	
4	1	5	10.888	11.523	11.540	11.540	9.7697
		10	9.7717	9.7697	9.7697	9.7697	
		15	9.7717	9.7697	9.7697	9.7697	
	2	5	23.685	26.034	26.064	26.064	26.161
		10	26.170	26.161	26.161	26.161	
		15	26.170	26.161	26.161	26.161	
	3	5	52.493	54.658	54.676	54.676	54.121
		10	54.220	54.121	54.121	54.121	
		15	54.220	54.121	54.121	54.121	
	4	5	87.056	85.469	85.461	85.461	83.939
		10	83.985	83.939	83.939	83.939	
		15	83.985	83.939	83.939	83.939	
	5	5	127.95	126.59	126.57	126.57	124.85
		10	124.50	124.85	124.85	124.85	
		15	124.50	124.85	124.85	124.85	
	6	5	167.09	168.51	168.68	168.69	167.13
		10	163.98	167.13	167.13	167.13	
		15	163.98	167.13	167.13	167.13	
8	1	5	9.8593	9.8602	9.8602	9.8602	9.7697
		10	9.7697	9.7697	9.7697	9.7697	
		15	9.7697	9.7697	9.7697	9.7697	
	2	5	26.191	26.192	26.192	26.191	26.161
		10	26.161	26.161	26.161	26.161	
		15	26.161	26.161	26.161	26.161	
	3	5	54.191	54.193	54.193	54.193	54.121
		10	54.121	54.121	54.121	54.121	
		15	54.121	54.121	54.121	54.121	
	4	5	84.011	84.014	84.014	84.014	83.939
		10	83.938	83.939	83.939	83.939	
		15	83.938	83.939	83.939	83.939	
	5	5	124.93	124.94	124.94	124.94	124.85
		10	124.84	124.85	124.85	124.85	
		15	124.84	124.85	124.85	124.85	
	6	5	167.13	167.20	167.20	167.20	167.13
		10	167.09	167.13	167.13	167.13	
		15	167.09	167.13	167.13	167.13	

where a and b are the length of the long and short axes, respectively. In Eq. (11),

$$\xi = \frac{1}{L}(a^2\cos^2\theta + b^2\sin^2\theta)^{1/2}. \tag{26}$$

The results were obtained by decomposing an arch into eight sub-domains, by using $n_c = n_s = 15$ to determine $N^{(0)}$ and using $n_c = 15$ and $n_s = 30$ to obtain the dynamic solution. Notably, a non-dimensional loading parameter $\beta = \chi L^3/EI$ and a slenderness parameter $\mu = L/\gamma$, where γ is the radius of gyration of a cross-section area, were introduced. The characteristic length L was chosen as $2a$.

Table 2
Non-dimensional frequency parameters λ for clamped elliptic arches subjected to the static load $\beta = 50$

μ	b/a	θ (°)	Mode					
			1	2	3	4	5	6
100	0.2	60	91.468	239.17	475.21	627.47	789.89	1181.2
		120	33.808	48.878	132.18	227.75	359.33	363.64
		180	15.351	24.603	99.702	141.61	247.42	280.08
	0.5	60	117.27	228.64	462.55	622.83	772.88	1149.3
		120	53.966	77.101	152.57	208.86	336.63	362.23
		180	24.448	41.313	102.39	130.56	225.45	227.11
	0.8	60	153.49	216.62	446.94	614.11	749.89	1104.1
		120	46.034	86.071	171.13	179.33	293.44	345.46
		180	14.670	35.643	75.471	115.58	176.97	197.33
20	0.2	60	89.066	125.39	245.23	250.97	376.62	478.28
		120	28.169	70.043	79.683	143.29	155.15	215.77
		180	20.618	50.731	63.291	102.98	122.11	167.94
	0.5	60	87.638	123.94	238.75	249.06	374.53	459.76
		120	28.526	58.654	77.235	129.94	143.30	205.64
		180	21.931	27.143	58.983	71.410	106.93	123.20
	0.8	60	85.571	121.22	228.30	245.54	370.29	435.83
		120	31.812	45.917	73.655	108.69	133.79	183.29
		180	15.006	25.716	87.581	91.755	133.15	136.48

Table 3
Non-dimensional frequency parameters λ for clamped elliptic arches subjected to the static load $\beta = -50$

μ	b/a	θ (°)	Mode					
			1	2	3	4	5	6
100	0.2	60	99.696	251.01	488.21	627.56	803.51	1195.0
		120	59.794	101.22	185.64	283.30	366.83	418.22
		180	56.233	75.220	148.09	194.25	303.25	304.34
	0.5	60	126.87	246.01	481.78	623.63	792.77	1169.1
		120	81.210	92.401	175.75	239.32	368.29	369.81
		180	45.194	60.046	125.33	149.93	245.45	248.07
	0.8	60	160.40	232.22	464.42	615.94	767.48	1122.3
		120	63.538	102.44	180.12	200.98	316.12	352.31
		180	29.053	51.334	93.950	133.44	196.99	205.89
20	0.2	60	89.452	125.39	245.68	250.97	376.62	478.72
		120	32.026	70.767	84.174	143.50	160.68	215.82
		180	23.116	53.318	63.861	106.04	122.16	170.86
	0.5	60	88.591	123.954	239.86	249.08	374.56	460.69
		120	35.149	63.176	83.518	134.51	150.66	206.41
		180	29.87	39.390	64.687	86.867	110.22	140.40
	0.8	60	87.048	121.29	230.05	245.62	370.41	437.26
		120	37.608	52.829	79.561	117.951	138.81	188.95
		180	26.737	31.060	56.593	64.456	95.264	103.61

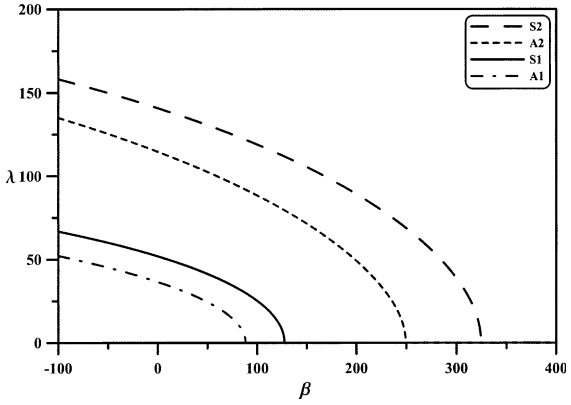

Fig. 3. Variation of λ with β for a clamped elliptic arch with $b/a = 0.5$, $\mu = 100$ and $\theta_0 = 180°$.

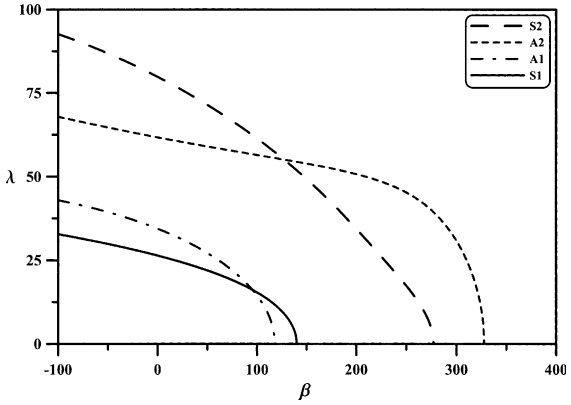

Fig. 4. Variation of λ with β for a clamped elliptic arch with $b/a = 0.5$, $\mu = 20$ and $\theta_0 = 180°$.

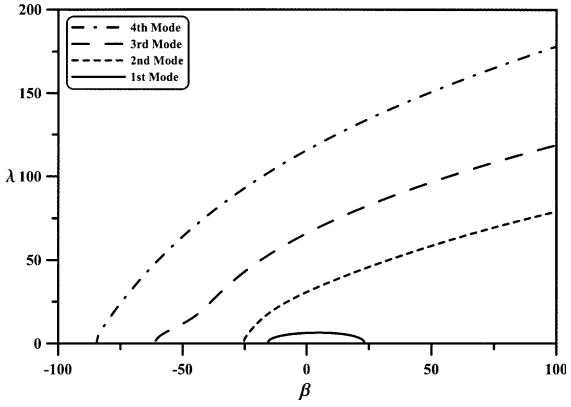

Fig. 5. Variation of λ with β for a fixed–free elliptic arch with $b/a = 0.5$, $\mu = 100$ and $\theta_0 = 180°$.

5.1. Natural frequencies

Tables 2 and 3 list the non-dimensional frequency parameters λ for clamped elliptic arches subjected to uniform vertical loading $\beta = 50$ and -50, respectively. Although a larger μ value represents a smaller thickness of the arch, the

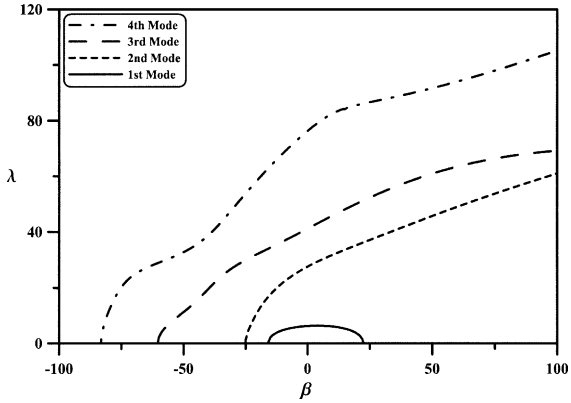

Fig. 6. Variation of λ with β for a fixed–free elliptic arch with $b/a = 0.5$, $\mu = 20$ and $\theta_0 = 180°$.

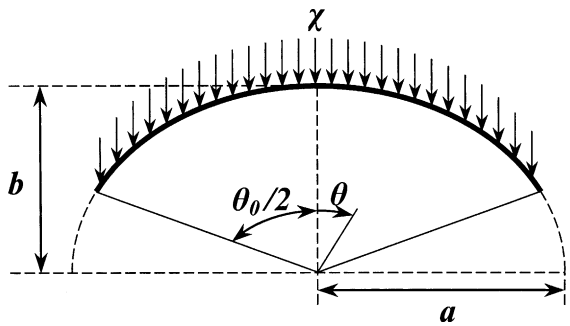

Fig. 7. Sketch of an elliptic arch subjected to vertical static loading.

frequency parameters λ increase as μ is increased because μ is involved in the definition of λ. As expected, λ decreases with increasing θ_0 because the stiffness of the arch decreases and the mass of the arch increases as θ_0 increases. The trend for the variation of the frequency parameters with b/a is not clear and depends on which θ_0, μ, and mode are considered.

Figs. 3 and 4 show the variation of λ with β for clamped elliptic arches with $\mu = 100$ and 20, respectively, while Figs. 5 and 6 depict the variation for cases with fixed–free boundary conditions. Arches with $a/b = 0.5$ and $\theta_0 = 180°$ were considered here. Figs. 3 and 4 indicate that different μ can lead to different variation patterns for λ versus β. In Fig. 4, it is observed that curves from different symmetric classes cross. For the cases with fixed–free boundary conditions, the trend for λ versus β is totally different from that for the clamped cases. Figs. 5 and 6 do not exhibit the trend where the values of λ monotonically decrease with the increase of β as shown in Figs. 3 and 4. Instead, for fixed–free arches, λ decreases with the decrease of β. Interestingly, positive and negative β can lead to arches that elastically buckle. The differences in the patterns of λ versus β for clamped and fixed–free arches can be explained by the distribution of $N^{(0)}$ caused by the uniformly distributed vertical loading (see Fig. 8). As shown in Fig. 8, when an arch is subjected to a vertical loading with positive β, the resulting axial forces are compressive for the clamped arch, while $N^{(0)}$ for the fixed–free arch can be compressive or tensile, depending on its position.

5.2. Buckling loads

Table 4 lists the buckling loads corresponding to the first two modes of clamped elliptic arches with various b/a, θ_0 and μ, while Fig. 9 depicts the variation of the buckling loads with θ_0 for the arches with $b/a = 0.5$. In Fig. 9, A1 and S1 denote the first anti-symmetric and symmetric modes, respectively. The mode shape for the lowest buckling load changes from symmetric to anti-symmetric as θ_0 is increased. These results suggest that the bucking loads decrease with the increase of θ_0 or μ because the bending stiffness of the arch becomes smaller as the arch become longer or more slender. However, there is no clear trend for the influence of b/a on the buckling loads. Finally, it should be noted that

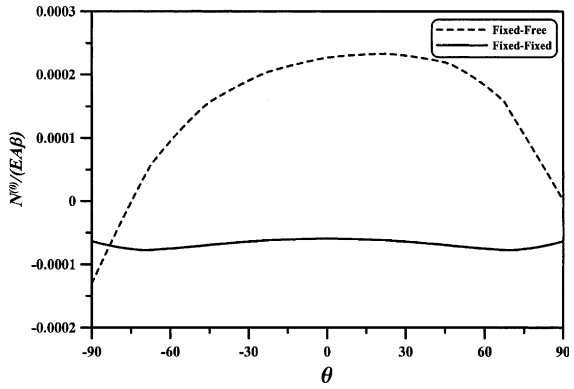

Fig. 8. Distribution of $N^{(0)}$ for elliptic arches with $b/a = 0.5$, $\mu = 100$ and $\theta_0 = 180°$.

Table 4
Non-dimensional buckling loads β for clamped elliptic arches

μ	b/a	θ_0 (°)	Mode	
			1	2
100	0.2	60	562.64	1014.2
		120	79.233	85.716
		180	54.102	65.602
	0.5	60	587.64	666.76
		120	125.69	187.31
		180	88.458	127.59
	0.8	60	697.85	897.10
		120	155.98	247.06
		180	82.816	138.05
20	0.2	60	11465	26719
		120	386.38	765.47
		180	421.63	780.29
	0.5	60	4563.3	10276
		120	234.49	333.04
		180	117.99	140.07
	0.8	60	2857.1	6033.3
		120	240.28	270.92
		180	88.826	148.07

the reported buckling loads are not related to snap-through buckling that may be important to very flat curved bars [16]. The proposed solution is not suitable for the snap-through response because the proposed solution neglects the deformation due to the static loads.

6. Concluding remarks

An analytical solution for the free vibration and stability of loaded arches with varying curvature has been developed by incorporating series solutions and stiffness matrixes. The equations of motion for small amplitude free vibrations about a pre-stressed static equilibrium state have been developed based on a variational principle and considering the extensibility of the arch centerline but ignoring shear deformation. The vibration frequencies and buckling loads of arches have been determined by establishing a static solution for the distribution of the axial force due to static external

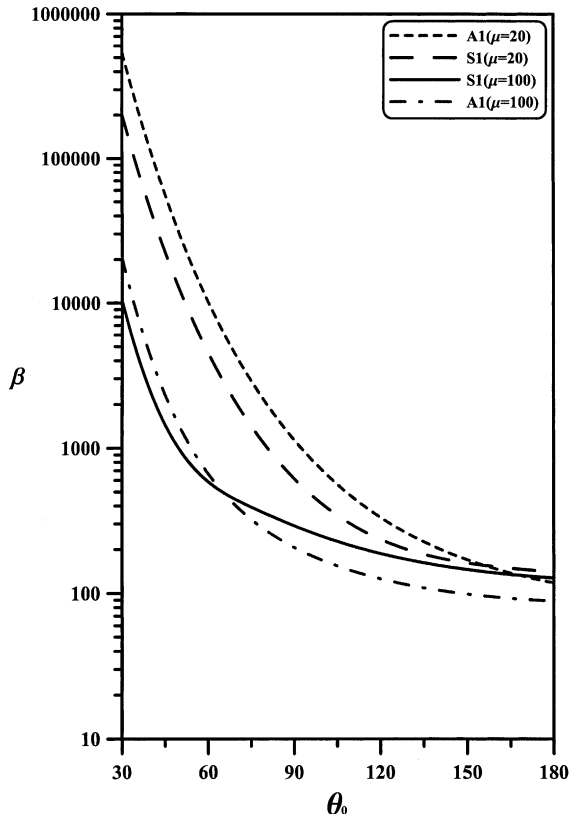

Fig. 9. Buckling loads for clamped elliptic arches with $b/a = 0.5$ and various θ_0 and μ.

forces and a dynamic solution for the free vibration. Both of the solutions have been developed by decomposing the arch under consideration into several elements, constructing a series solution of governing equations defined in each element, and, finally, establishing element-wise stiffness matrixes from the series solutions to form a global stiffness matrix.

The proposed solution has been validated through convergence studies and comparison of the present results with published data on the vibration frequencies of circular arches subjected to uniformly distributed vertical forces. The solution has also been applied to determine the vibration frequencies and buckling loads of fixed–fixed and fixed–free elliptic arches with various b/a, θ_0 and μ. The arches were subjected to static vertical forces with uniform distribution. The non-dimensional frequency parameters λ and the magnitude of the buckling loads were found to decrease with the increase of θ_0 and with the decrease of μ, while there was no definite trend for λ or for the bucking loads varying with b/a. The parameters λ were also found to decrease with the increase of the non-dimensional loading parameters β for clamped elliptic arches, while different trends were observed for fixed–free arches because the distributions of initial axial forces are very different for arches with these two different boundary conditions. Consequently, only positive β was found to cause the clamped arches to buckle, while both negative β and positive β caused fixed–free arches to buckle.

The present solution can be used to analyze the in-plane free vibration and stability of any types of arch with various static external forces. Furthermore, the proposed solution procedure can be easily modified and used to determine the transient responses of loaded arches by introducing Laplace transform into the dynamic solution [17]. One can also introduce Fourier transform into the dynamic solution to analyze stationary random vibration problems of loaded arches.

Acknowledgement

The research reported herein was supported by the National Science Council, ROC (NSC 90-2211-E-009-035). This support is gratefully acknowledged.

Appendix A. The expression for $[\widehat{\boldsymbol{K}}_n]$ and $\{\boldsymbol{f}_n^{(p)}\}$

$$[\widehat{\boldsymbol{K}}_n] = [\alpha_n][\beta_n]^{-1}, \tag{A.1}$$

where

$$[\alpha_n] = [\alpha_n]_1 + [\alpha_n]_2 + [\alpha_n]_3 + [\alpha_n]_4 + [\alpha_n]_5 + [\alpha_n]_6 + [\alpha_n]_7, \tag{A.2}$$

$$[\alpha_n]_1 = -\frac{EI\xi^3}{L^2}\begin{bmatrix} 0 & 0 & 0 & 0 & 0 & 0 \\ -\hat{w}_0'''(\theta_n) & -\hat{w}_1'''(\theta_n) & -\hat{w}_2'''(\theta_n) & -\hat{w}_3'''(\theta_n) & -\hat{w}_4'''(\theta_n) & -\hat{w}_5'''(\theta_n) \\ 0 & 0 & 0 & 0 & 0 & 0 \\ 0 & 0 & 0 & 0 & 0 & 0 \\ \hat{w}_0'''(\theta_{n+1}) & \hat{w}_1'''(\theta_{n+1}) & \hat{w}_2'''(\theta_{n+1}) & \hat{w}_3'''(\theta_{n+1}) & \hat{w}_4'''(\theta_{n+1}) & \hat{w}_5'''(\theta_{n+1}) \\ 0 & 0 & 0 & 0 & 0 & 0 \end{bmatrix}, \tag{A.3}$$

$$[\alpha_n]_2 = \frac{EI\xi^2}{L}\begin{bmatrix} 0 & 0 & 0 & 0 & 0 & 0 \\ 0 & \frac{3\xi'}{L} & 0 & 0 & 0 & 0 \\ 0 & 0 & -1 & 0 & 0 & 0 \\ 0 & 0 & 0 & 0 & 0 & 0 \\ 0 & 0 & 0 & 0 & -\frac{3\xi'}{L} & 0 \\ 0 & 0 & 0 & 0 & 0 & 1 \end{bmatrix}\begin{bmatrix} 0 & 0 & 0 & 0 & 0 & 0 \\ \hat{w}_0''(\theta_n) & \hat{w}_1''(\theta_n) & \hat{w}_2''(\theta_n) & \hat{w}_3''(\theta_n) & \hat{w}_4''(\theta_n) & \hat{w}_5''(\theta_n) \\ \hat{w}_0''(\theta_n) & \hat{w}_1''(\theta_n) & \hat{w}_2''(\theta_n) & \hat{w}_3''(\theta_n) & \hat{w}_4''(\theta_n) & \hat{w}_5''(\theta_n) \\ 0 & 0 & 0 & 0 & 0 & 0 \\ \hat{w}_0''(\theta_{n+1}) & \hat{w}_1''(\theta_{n+1}) & \hat{w}_2''(\theta_{n+1}) & \hat{w}_3''(\theta_{n+1}) & \hat{w}_4''(\theta_{n+1}) & \hat{w}_5''(\theta_{n+1}) \\ \hat{w}_0''(\theta_{n+1}) & \hat{w}_1''(\theta_{n+1}) & \hat{w}_2''(\theta_{n+1}) & \hat{w}_3''(\theta_{n+1}) & \hat{w}_4''(\theta_{n+1}) & \hat{w}_5''(\theta_{n+1}) \end{bmatrix}, \tag{A.4}$$

$$[\alpha_n]_3 = \frac{EI\xi}{L}\begin{bmatrix} 0 & 0 & 0 & 0 & 0 & 0 \\ 0 & \frac{\xi''\xi+(\xi')^2}{L} & 0 & 0 & 0 & 0 \\ 0 & 0 & -\xi' & 0 & 0 & 0 \\ 0 & 0 & 0 & 0 & 0 & 0 \\ 0 & 0 & 0 & 0 & -\frac{\xi''\xi+(\xi')^2}{L} & 0 \\ 0 & 0 & 0 & 0 & 0 & \xi' \end{bmatrix} \times \begin{bmatrix} 0 & 0 & 0 & 0 & 0 & 0 \\ \hat{w}_0'(\theta_n) & \hat{w}_1'(\theta_n) & \hat{w}_2'(\theta_n) & \hat{w}_3'(\theta_n) & \hat{w}_4'(\theta_n) & \hat{w}_5'(\theta_n) \\ \hat{w}_0'(\theta_n) & \hat{w}_1'(\theta_n) & \hat{w}_2'(\theta_n) & \hat{w}_3'(\theta_n) & \hat{w}_4'(\theta_n) & \hat{w}_5'(\theta_n) \\ 0 & 0 & 0 & 0 & 0 & 0 \\ \hat{w}_0'(\theta_{n+1}) & \hat{w}_1'(\theta_{n+1}) & \hat{w}_2'(\theta_{n+1}) & \hat{w}_3'(\theta_{n+1}) & \hat{w}_4'(\theta_{n+1}) & \hat{w}_5'(\theta_{n+1}) \\ \hat{w}_0'(\theta_{n+1}) & \hat{w}_1'(\theta_{n+1}) & \hat{w}_2'(\theta_{n+1}) & \hat{w}_3'(\theta_{n+1}) & \hat{w}_4'(\theta_{n+1}) & \hat{w}_5'(\theta_{n+1}) \end{bmatrix}, \tag{A.5}$$

$$[\alpha_n]_4 = \frac{EA}{R}\begin{bmatrix} -\hat{w}_0(\theta_n) & -\hat{w}_1(\theta_n) & -\hat{w}_2(\theta_n) & -\hat{w}_3(\theta_n) & -\hat{w}_4(\theta_n) & -\hat{w}_5(\theta_n) \\ 0 & 0 & 0 & 0 & 0 & 0 \\ 0 & 0 & 0 & 0 & 0 & 0 \\ \hat{w}_0(\theta_{n+1}) & \hat{w}_1(\theta_{n+1}) & \hat{w}_2(\theta_{n+1}) & \hat{w}_3(\theta_{n+1}) & \hat{w}_4(\theta_{n+1}) & \hat{w}_5(\theta_{n+1}) \\ 0 & 0 & 0 & 0 & 0 & 0 \\ 0 & 0 & 0 & 0 & 0 & 0 \end{bmatrix}, \tag{A.6}$$

$$[\alpha_n]_5 = \frac{EI\xi^2}{L^2\bar{R}}\begin{bmatrix} 0 & 0 & 0 & 0 & 0 & 0 \\ -\hat{v}_0''(\theta_n) & -\hat{v}_1''(\theta_n) & -\hat{v}_2''(\theta_n) & -\hat{v}_3''(\theta_n) & -\hat{v}_4''(\theta_n) & -\hat{v}_5''(\theta_n) \\ 0 & 0 & 0 & 0 & 0 & 0 \\ 0 & 0 & 0 & 0 & 0 & 0 \\ \hat{v}_0''(\theta_{n+1}) & \hat{v}_1''(\theta_{n+1}) & \hat{v}_2''(\theta_{n+1}) & \hat{v}_3''(\theta_{n+1}) & \hat{v}_4''(\theta_{n+1}) & \hat{v}_5''(\theta_{n+1}) \\ 0 & 0 & 0 & 0 & 0 & 0 \end{bmatrix}, \tag{A.7}$$

$$[\alpha_n]_6 = E\xi \begin{bmatrix} -A & 0 & 0 & 0 & 0 & 0 \\ 0 & \frac{I}{L^2}\left(\frac{2\xi\bar{R}'-\xi'\bar{R}}{\bar{R}^2}\right) & 0 & 0 & 0 & 0 \\ 0 & 0 & \frac{I}{L\bar{R}} & 0 & 0 & 0 \\ 0 & 0 & 0 & A & 0 & 0 \\ 0 & 0 & 0 & 0 & -\frac{I}{L^2}\left(\frac{2\xi\bar{R}'-\xi'\bar{R}}{\bar{R}^2}\right) & 0 \\ 0 & 0 & 0 & 0 & 0 & -\frac{I}{L\bar{R}} \end{bmatrix}$$
$$\times \begin{bmatrix} \hat{v}_0'(\theta_n) & \hat{v}_1'(\theta_n) & \hat{v}_2'(\theta_n) & \hat{v}_3'(\theta_n) & \hat{v}_4'(\theta_n) & \hat{v}_5'(\theta_n) \\ \hat{v}_0'(\theta_n) & \hat{v}_1'(\theta_n) & \hat{v}_2'(\theta_n) & \hat{v}_3'(\theta_n) & \hat{v}_4'(\theta_n) & \hat{v}_5'(\theta_n) \\ \hat{v}_0'(\theta_n) & \hat{v}_1'(\theta_n) & \hat{v}_2'(\theta_n) & \hat{v}_3'(\theta_n) & \hat{v}_4'(\theta_n) & \hat{v}_5'(\theta_n) \\ \hat{v}_0'(\theta_{n+1}) & \hat{v}_1'(\theta_{n+1}) & \hat{v}_2'(\theta_{n+1}) & \hat{v}_3'(\theta_{n+1}) & \hat{v}_4'(\theta_{n+1}) & \hat{v}_5'(\theta_{n+1}) \\ \hat{v}_0'(\theta_{n+1}) & \hat{v}_1'(\theta_{n+1}) & \hat{v}_2'(\theta_{n+1}) & \hat{v}_3'(\theta_{n+1}) & \hat{v}_4'(\theta_{n+1}) & \hat{v}_5'(\theta_{n+1}) \\ \hat{v}_0'(\theta_{n+1}) & \hat{v}_1'(\theta_{n+1}) & \hat{v}_2'(\theta_{n+1}) & \hat{v}_3'(\theta_{n+1}) & \hat{v}_4'(\theta_{n+1}) & \hat{v}_5'(\theta_{n+1}) \end{bmatrix}, \tag{A.8}$$

$$[\alpha_n]_7 = \frac{EI\xi}{L\bar{R}^2} \begin{bmatrix} 0 & 0 & 0 & 0 & 0 & 0 \\ 0 & \frac{\bar{R}^2(\bar{R}''\xi+\bar{R}'\xi')-2\bar{R}(\bar{R}')^2\xi}{L\bar{R}^2} & 0 & 0 & 0 & 0 \\ 0 & 0 & -\bar{R}' & 0 & 0 & 0 \\ 0 & 0 & 0 & 0 & 0 & 0 \\ 0 & 0 & 0 & 0 & -\frac{\bar{R}^2(\bar{R}''\xi+\bar{R}'\xi')-2\bar{R}(\bar{R}')^2\xi}{L\bar{R}^2} & 0 \\ 0 & 0 & 0 & 0 & 0 & \bar{R}' \end{bmatrix}$$
$$\times \begin{bmatrix} 0 & 0 & 0 & 0 & 0 & 0 \\ \hat{v}_0(\theta_n) & \hat{v}_1(\theta_n) & \hat{v}_2(\theta_n) & \hat{v}_3(\theta_n) & \hat{v}_4(\theta_n) & \hat{v}_5(\theta_n) \\ \hat{v}_0(\theta_n) & \hat{v}_1(\theta_n) & \hat{v}_2(\theta_n) & \hat{v}_3(\theta_n) & \hat{v}_4(\theta_n) & \hat{v}_5(\theta_n) \\ 0 & 0 & 0 & 0 & 0 & 0 \\ \hat{v}_0(\theta_{n+1}) & \hat{v}_1(\theta_{n+1}) & \hat{v}_2(\theta_{n+1}) & \hat{v}_3(\theta_{n+1}) & \hat{v}_4(\theta_{n+1}) & \hat{v}_5(\theta_{n+1}) \\ \hat{v}_0(\theta_{n+1}) & \hat{v}_1(\theta_{n+1}) & \hat{v}_2(\theta_{n+1}) & \hat{v}_3(\theta_{n+1}) & \hat{v}_4(\theta_{n+1}) & \hat{v}_5(\theta_{n+1}) \end{bmatrix}. \tag{A.9}$$

$$\{\boldsymbol{f}_n^{(p)}\} = -[\widehat{\boldsymbol{K}}_n]\{\boldsymbol{D}_n^{(p)}\} + \{\boldsymbol{F}_n^{(p)}\}, \tag{A.10}$$

where

$$\{\boldsymbol{F}_n^{(p)}\} = \begin{Bmatrix} -N^{(p)}(\theta_n) \\ -Q^{(p)}(\theta_n) \\ -M^{(p)}(\theta_n) \\ N^{(p)}(\theta_{n+1}) \\ Q^{(p)}(\theta_{n+1}) \\ M^{(p)}(\theta_{n+1}) \end{Bmatrix}, \tag{A.11}$$

$$N^{(p)}(\theta) = EA\left[\frac{\hat{w}_p(\theta)}{\bar{R}(\theta)} + \xi(\theta)\hat{v}_p'(\theta)\right], \tag{A.12}$$

$$\begin{aligned} Q^{(p)}(\theta) = \frac{EI}{L^2}\Bigg\{ & -\xi^3(\theta)\hat{w}_p'''(\theta) - 3\xi^2(\theta)\xi'(\theta)\hat{w}_p''(\theta) - [\xi''(\theta)\xi^2(\theta) + (\xi'(\theta))^2\xi(\theta)]\hat{w}_p'(\theta) + \frac{\xi^2(\theta)}{\bar{R}(\theta)}\hat{v}_p''(\theta) \\ & - \frac{2\xi^2(\theta)\bar{R}'(\theta) - \xi'(\theta)\xi(\theta)\bar{R}(\theta)}{\bar{R}^2(\theta)}\hat{v}_p'(\theta) - \frac{\bar{R}^2(\theta)\xi(\theta)[\bar{R}''(\theta)\xi(\theta) + \bar{R}'(\theta)\xi'(\theta)] - 2\bar{R}(\theta)(\bar{R}'(\theta))^2\xi^2(\theta)}{\bar{R}^4(\theta)}\hat{v}_p(\theta)\Bigg\}, \end{aligned} \tag{A.13}$$

$$M^{(p)}(\theta) = \frac{EI}{L}\left\{\xi^2(\theta)\hat{w}_p''(\theta) + \xi'(\theta)\xi(\theta)\hat{w}_p'(\theta) - \frac{\xi(\theta)}{\bar{R}(\theta)}\hat{v}_p'(\theta) + \frac{\bar{R}'(\theta)\xi(\theta)}{\bar{R}^2(\theta)}\hat{v}_p(\theta)\right\}. \tag{A.14}$$

References

[1] Love AEH. Treatise on the mathematical theory of elasticity. New York: Dover; 1944.
[2] Markus S, Nanasi T. Vibration of curved beams. Shock Vib Dig 1981;13(4):3–14.
[3] Laura PAA, Maurizi MJ. Recent research on vibrations of arch-type structures. Shock Vib Dig 1987;19(1):6–9.
[4] Chidamparam P, Leissa AW. Vibrations of planar curved beams, rings, and arches. Appl Mech Rev 1993;46(9):467–83.
[5] Timoshenko S, Gere JM. Theory of elastic stability. New York: McGraw-Hill; 1961.
[6] Simitses GJ. An introduction to the elastic stability of structures. New Jersey: Prentice-Hall; 1976.
[7] Gjelsvik A, Bodner SR. Energy criterion and snap buckling of arches. J Engng Mech Div, ASCE 1962;88(EM5):87–134.
[8] Schreyer HL, Masur EF. Buckling of shallow arches. J Engng Mech Div, ASCE 1966;92(EM4):1–17.
[9] Wasserman Y. The influence of the behaviour of the load on the frequencies and critical loads of arches with flexibility supported ends. J Sound Vib 1977;54:515–26.
[10] Kang KL, Bert CW, Striz AG. Vibration and buckling analysis of circular arches using DQM. Comput Struct 1996;60(1):49–57.
[11] Lin JL, Soedel W. General in-plane vibrations of rotating thick and thin rings. J Sound Vib 1988;122:547–70.
[12] Chidamparam P, Leissa AW. Influence of centerline extensibility on the in-plane free vibrations of loaded circular arches. J Sound Vib 1995;183(5):779–95.
[13] Huang CS, Nieh KY. An analytical solution for vibrations of loaded circular arches. In: Proceedings of the 6th Structural Engineering, Ping-Tung, Taiwan, 2002 [in Chinese].
[14] Washizu K. Variational methods in elasticity and plasticity. Oxford: Pergamon Press; 1982.
[15] Reddy JN. Energy and variational methods in applied mechanics. New York: John Wiley; 1984.
[16] Timoshenko SP, Gere JM. Theory of elastic stability. 2nd ed. New York: McGraw-Hill; 1961.
[17] Huang CS, Tseng YP, Lin CR. In-plane transient responses of an arch with variable curvature. J Engng Mech, ASCE 1998;124(8):826–35.